1   # Enhanced SARS-CoV-2 Neutralization by Secretory IgA in vitro

2

3   Zijun Wang[1,†], Julio C. C. Lorenzi[1,†], Frauke Muecksch[2,†], Shlomo Finkin[1,†], Charlotte Viant[1],

4   Christian Gaebler[1], Melissa Cipolla[1], Hans-Heinrich Hoffman[3], Thiago Y. Oliveira[1], Deena A.

5   Oren[4], Victor Ramos[1], Lilian Nogueira[1], Eleftherios Michailidis[3], Davide F. Robbiani[5], Anna

6   Gazumyan[1], Charles M. Rice[3], Theodora Hatziioannou[2], Paul D. Bieniasz[2,6], Marina Caskey[1],

7   Michel C. Nussenzweig[1,6,*].

8

9   [1] Laboratory of Molecular Immunology, The Rockefeller University, New York, NY, USA.

10   [2] Laboratory of Retrovirology, The Rockefeller University, New York, NY, USA.

11   [3] Laboratory of Virology and Infectious Disease, The Rockefeller University, New York, NY,

12   USA.

13   [4] Structural Biology Resource Center, The Rockefeller University, New York, NY 10065, USA

14   [5] Institute for Research in Biomedicine, Università della Svizzera italiana, Bellinzona,

15   Switzerland.

16   [6] Howard Hughes Medical Institute, The Rockefeller University, New York, NY, USA.

17   [†] Equal contributions

18   [*] **Correspondence to:** nussen@rockefeller.edu**(M.C.N)**

19

20

21

22

23   **Abstract:** SARS-CoV-2 primarily infects cells at mucosal surfaces. Serum neutralizing antibody

24   responses are variable and generally low in individuals that suffer mild forms of the illness.

25   Although potent IgG antibodies can neutralize the virus, less is known about secretory antibodies

26   such as IgA that might impact the initial viral spread and transmissibility from the mucosa. Here

27   we characterize the IgA response to SARS-CoV-2 in a cohort of 149 individuals. IgA responses

28   in plasma generally correlate with IgG responses and clones of IgM, IgG and IgA producing B

29   cells that are derived from common progenitors are evident. Plasma IgA monomers are 2-fold

30   less potent than IgG equivalents. However, IgA dimers, the primary form in the nasopharynx, are

31   on average 15 times more potent than IgA monomers. Thus, secretory IgA responses may be

32   particularly valuable for protection against SARS-CoV-2 and for vaccine efficacy.

33

34   **Introduction**

35   SARS-CoV-2 encodes a trimeric spike surface protein (S) which mediates entry into host cells

36   (*1, 2*). The virus initially infects epithelial cells in the nasopharynx when the receptor binding

37   domain (RBD) of S interacts with angiotensin converting enzyme-2 (ACE-2) receptor (*3-6*).

38   SARS-CoV-2 may subsequently spread to other epithelial cells expressing ACE-2 in the lung

39   and gut. These tissues are rich in lymphoid cells that are organized into nasopharynx associated

40   and gut associated lymphoid tissues (NALT and GALT respectively). Vaccines delivered by

41   inhalation to specifically target these tissues appear to be more effective against SARS-CoV-2

42   (*7*). Among other specializations, NALT and GALT produce large quantities of IgA antibodies.

43   These antibodies exist as monomers in circulation where they make up 15% of the serum

44   antibody pool. However, IgA is found in higher concentrations in secretions where it exists

45   predominantly as a dimer covalently linked by J chain (*8-10*).

46

Although most individuals produce antibodies in response to SARS-CoV-2 infection, the

neutralizing response is highly variable with as many as 30% of the population showing levels of

neutralizing activity below 1:50 in pseudovirus assays (*11, 12*). Neutralization is associated with

prolonged infection and RBD binding activity as measured by ELISA (*11-13*). IgG antibody

cloning experiments from recovered individuals have revealed that neutralizing antibodies target

several distinct non-overlapping epitopes on the RBD (*11, 14-18*). Some of these antibodies are

potently neutralizing and can prevent or treat infection in animal models (*15-19*).

Consistent with the fact that SARS CoV-2 initially infects in the nasopharynx, IgA antibodies

that bind to SARS-CoV-2 are produced rapidly after infection and remain elevated in the plasma

for at least 40 days after the onset of symptoms (*20-23*). IgA antibodies bind to the RBD and can

neutralize SARS-CoV-2 (*20-22*). However, the precise contribution and molecular nature of the

IgA response to SARS-CoV-2 has not been reported to date. Here we examine a cohort of 149

convalescent individuals with measurable plasma neutralizing activity for the contribution of IgA

to anti-SARS-CoV-2 antibody responses. Cloning IgA antibodies from single B cells reveals that

the neutralizing activity of monomeric IgA is generally lower than corresponding IgGs but

dimeric IgAs are on average 15-fold more potent than their monomeric counterparts.

Results

Plasma anti-SARS-CoV-2 RBD IgA

IgM, IgG and IgA account for 5%, 80% and 15% of the antibodies in plasma, respectively. IgG

responses to RBD are strongly correlated with neutralizing activity (*11, 13-17, 24-28*). To

69   examine the contribution of IgA to the anti-SARS-CoV-2 RBD response we tested plasma

70   samples for binding to the RBD by a validated ELISA. A positive control sample (COV-21) was

71   included for normalization of the area under the curve (AUC) and 8 independent healthy donor

72   samples were included as negative controls (Fig. 1A, (*11*)). Whereas 78% and 15% of the

73   individuals in this cohort showed IgG and IgM anti-RBD levels that were at least 2 standard

74   deviations above control, only 33% did so for IgA (Fig. 1A and B, (*11*)). Thus, in individuals

75   studied on average 40 days after infection the circulating levels of anti-RBD IgA is more modest

76   than IgG and higher than IgM.

77

78   Anti-RBD IgA titers were correlated with duration and severity of symptoms but not timing of

79   sample collection relative to onset (Fig. 1C, and fig.S1A, B). Similar to IgG, females had lower

80   levels of IgA than males and hospitalized individuals showed higher anti-RBD IgA titers than

81   those with milder symptoms, but there was no correlation with age (Fig. 1D and E, fig. S1C). Of

82   note, individuals that suffered gastrointestinal symptoms showed significantly higher plasma

83   anti-RBD IgA but not IgG titers (Fig. 1F and fig. S1D).

84

85   **Neutralization activity of purified IgG and IgA**

86   To compare the neutralizing activity of plasma IgA to IgG directly we purified the 2 isotypes

87   from the plasma of all 99 individuals in our cohort that showed measurable plasma neutralizing

88   activity and tested the two isotypes in HIV-1 based SARS-CoV-2 pseudovirus neutralization

89   assays (*11*). The activity of both isotypes was directly correlated with anti-RBD binding titers

90   and overall plasma neutralizing activity (Fig. 2A-D). In addition, there was good correlation

91   between the neutralizing activity of IgG and IgA in a given individual (Fig. 2E). However,

92   potency of each of the 2 isotypes varied by as much as 2 orders of magnitude between

93   individuals (Fig. 2F). Purified IgG was generally more potent than IgA in neutralizing SARS-

94   CoV-2 pseudovirus *in vitro*. The geometric mean IC_{50} for IgG was 384 nM vs. 709 nM for IgA

95   ($P < 0.0001$, Fig. 2F). Nevertheless, IgAs were more potent than IgGs in 25% of the individuals

96   tested (fig. S2A). The 2 isotypes also differed in that the overall potency of purified IgG was

97   correlated with symptom severity and was higher in hospitalized individuals, but purified IgA

98   was not (Fig. 2G and fig. S2B- D). Finally, the potency of the purified IgA was greater in

99   individuals that suffered from gastrointestinal symptoms, but IgG was not (Fig. 2H and fig. S2E).

100

101 **Monoclonal anti-SARS-CoV-2 IgM and IgA antibodies**

102 To determine the nature of the IgM and IgA anti-RBD antibodies elicited by SARS-CoV-2

103 infection we used flow cytometry to purify single B lymphocytes that bind to RBD and cloned

104 their antibodies. We obtained 109 IgM and 74 IgA (64 IgA1 and 10 IgA2) matched Ig heavy and

105 light chain sequences by reverse transcription and subsequent isotype specific PCR from 3

106 convalescent individuals (Fig. 3A, B). As reported for IgG antibodies (*11, 14, 17, 26, 29*), the

107 overall number of mutations was generally low when compared to antibodies obtained from

108 individuals suffering from chronic infections such as Hepatitis-B or HIV-1 (*30, 31*) (fig. S3A,

109 B). However, the number of V gene nucleotide mutations in IgM and IgA heavy and light chains

110 varied between individuals. For example, in donor COV21 the number of IgM and IgA heavy

111 chain mutations was similar. In contrast, IgM heavy and light chain nucleotide mutations were

112 significantly greater than IgA mutations in COV47 (fig. S3B). CDR3 length was significantly

113 shorter for IgM than IgA and IgG antibodies and hydrophobicity was slightly higher for IgM

114 over control but not for IgA and IgG (figs. S4 and S5). Compared to the normal human antibody

115   repertoire, several IgA and IgM VH genes were over-represented including VH3-53 which can

116   make key contacts with the RBD through germline encoded CDRH1 and CDRH2 (*11, 32, 33*)

117   (fig. S6).

118

119   Like IgG antibodies (*11*) IgA and IgM antibodies were found in expanded clones in all 3 of the

120   individuals examined. Overall 66.2% and 66.1% of all the IgA and IgM sequences examined

121   were members of expanded clones (Fig. 3A, B and table S1). Nearly identical sequences were

122   shared among the 3 isotypes in clones found in all 3 individuals indicating that switch

123   recombination occurred during B cell clonal expansion in response to SARS-CoV-2 (Fig.3B). In

124   total 11 out of 55 antigen-specific B cell clones in circulation belonged to expanded clones that

125   contained members expressing different constant regions (Fig. 3C and tables S1 and S2). When

126   compared directly, the neutralizing activity of antibodies that were members of B cell clones

127   producing IgA or IgG varied and did not correlate with one or the other isotype (table S3).

128

129   To examine the binding properties of the anti-SARS-CoV-2 monoclonals we expressed 46 IgMs

130   and 35 IgAs (table S4). IgM variable regions were produced on an IgG1 backbone to facilitate

131   expression and purification. IgAs were expressed as native IgA1 or IgA2 monomers. ELISA

132   assays on RBD showed that 100% and 91.3% of the IgA and IgM antibodies bound to the RBD

133   with an average half-maximal effective concentration of 52.8 ng/ml and 101.6 ng/ml respectively

134   (fig. S7A and table S5).

135

136   To determine neutralizing activity of the IgM and IgA antibodies we tested them against an HIV-

137   1 based SARS-CoV-2 pseudovirus as IgGs and native IgA monomers respectively. Among the

138 42 RBD binding IgM antibodies tested we found 10 that neutralized the virus in the ng/ml range

139 with geometric mean half-maximal inhibitory concentrations (IC_{50}) of 114.0 nanograms per

140 milliliter (Fig. 4A and fig. S7B, table S5). In contrast, 32 out of 35 RBD binding IgA antibodies

141 tested neutralized the virus in the ng/ml range with geometric mean half-maximal inhibitory

142 concentrations (IC_{50}) of 53.6 nanograms per milliliter (Fig. 4A and fig. S7B, table S5). Thus,

143 IgM antibodies expressed as monomeric IgGs show lower neutralizing activity than either native

144 IgA or IgG monomers (Fig. 4A).

145

146 **Dimeric anti- SARS-CoV-2 IgA is more potent than monomeric IgA**

147 To determine whether these IgAs targeted the same epitopes as previously characterized IgGs we

148 performed bilayer interferometry experiments in which a preformed antibody-RBD complex

149 consisting of C144-RBD, or C121-RBD or C135-RBD or CR3022-RBD (Fig. 4B) was exposed

150 to a monomeric IgA monoclonal. C144 and C121 recognize the ACE-2 interaction domain of the

151 RBD, C135 and CR3022 neutralize without interfering with ACE-2 binding (Fig. 4C) (*11, 32,*

152 *34*). Two of the IgA's were in the C144 category, 5 were similar to C121, and 2 resembled C135

153 (Fig. 4C and fig. S9). Thus, RBD recognition by neutralizing IgA is similar to IgG.

154

155 Mucosal IgA exists predominantly as a dimer. To examine the neutralizing activity of IgA

156 dimers we co-expressed 8 IgA1s and 1 IgA2 with J chain to produce mixtures of monomers and

157 dimers that were purified by size exclusion chromatography (fig. S8). When compared in

158 pseudovirus neutralization assays, 8 out of 9 IgA dimers were more potent than the

159 corresponding monomers with differences in activity ranging from 3.8 to 113-fold (Fig. 4D, fig.

160 S10A and table S6). The relative increase in neutralizing activity between monomer and dimer

161   was inversely correlated with the neutralizing activity of the monomer in this assay (fig. S10B.

162   IC$_{50}$: r=0.80, P=0.014). For example, whereas C437, the most potent antibody, showed

163   equivalent activity as a monomer and dimer, C408, one of the least potent antibodies, was 113-

164   fold more potent as a dimer (fig. S10B).

165

166   IgA monomers and dimers were also compared in SARS-CoV-2 microneutralization assays.

167   Neutralizing activities of the 9 monomers and 9 dimers correlated strongly with those measured

168   in the pseudovirus neutralization assay (fig. S10C. IC$_{50}$: r=0.84, P<0.0001; IC$_{90}$: r=0.91,

169   P<0.0001). On average, there was a 15-fold geometric mean increase in activity for the dimer

170   over the monomer against SARS-CoV-2 and less variability in the degree of enhancement in

171   microneutralization compared to pseudovirus assays (Fig. 4D, fig. S10D and E, and table S6).

172   Thus, dimeric IgA is far more potent than monomeric IgA against SARS-CoV-2 (Fig. 4D).

173

174   **Discussion**

175   Neutralizing antibody titers are the best correlates of protection in most vaccines (*35*). Among

176   antibody isotypes, secretory IgA which is found at mucosal surfaces, plays a crucial role in

177   protecting against pathogens that target these surfaces (*36*). We find that serum IgA responses to

178   SARS-CoV-2 correlate with IgG responses. Although the monomeric form of IgA found in

179   serum is on average 2-fold less potent than IgG, the dimeric secretory form of IgA found in

180   mucosa is over one log more potent than the monomer against authentic SARS-CoV-2 which

181   makes it a far more potent neutralizer than IgG.

182

183 The increased potency of the dimeric form of IgA suggests that crosslinking the S protein on the

184 viral surface enhances neutralizing activity either directly or simply through increased apparent

185 affinity. This observation is consistent with the finding that monovalent Fab fragments of serum

186 IgG antibodies are far less potent than the intact antibody (*32*). Whether this effect is due to

187 inter- or intra-spike crosslinking is not known, but it indicates that antibodies or drugs designed

188 to block entry by binding to the RBD could be made more potent by increasing their valency.

189

190 A number of different candidate vaccines to SARS-CoV-2 are currently being evaluated in the

191 clinic. Secretory IgA responses may be particularly important to these efforts in that potent

192 dimeric forms of these antibodies are found at the mucosal surfaces where cells are initially

193 targeted by SARS-CoV-2. Thus, even vaccines that elicit modest neutralizing activity in serum

194 may be protective because the secretory polymeric forms of antibodies in mucosa can neutralize

195 the virus. Vaccines that are specifically designed to elicit mucosal IgA responses may be

196 particularly effective preventing SARS-CoV-2 infection (*7*).

197

Reference and notes

198 **Reference and notes**

199 1. A. C. Walls *et al.*, Structure, Function, and Antigenicity of the SARS-CoV-2 Spike

200 Glycoprotein. *Cell* **181**, 281-292 e286 (2020).

201 2. P. Zhou *et al.*, A pneumonia outbreak associated with a new coronavirus of probable bat

202 origin. *Nature* **579**, 270-273 (2020).

203 3. M. Hoffmann *et al.*, SARS-CoV-2 Cell Entry Depends on ACE2 and TMPRSS2 and Is

204 Blocked by a Clinically Proven Protease Inhibitor. *Cell* **181**, 271-280 e278 (2020).

205   4.   R. Lu *et al.*, Genomic characterisation and epidemiology of 2019 novel coronavirus:
206   implications for virus origins and receptor binding. *Lancet* **395**, 565-574 (2020).

207   5.   D. Wrapp *et al.*, Cryo-EM structure of the 2019-nCoV spike in the prefusion
208   conformation. *Science* **367**, 1260-1263 (2020).

209   6.   J. Lan *et al.*, Structure of the SARS-CoV-2 spike receptor-binding domain bound to the
210   ACE2 receptor. *Nature* **581**, 215-220 (2020).

211   7.   A. O. Hassan *et al.*, A single-dose intranasal ChAd vaccine protects upper and lower
212   respiratory tracts against SARS-CoV-2. *Cell*, (2020).

213   8.   B. J. Underdown, J. M. Schiff, Immunoglobulin A: strategic defense initiative at the
214   mucosal surface. *Annu Rev Immunol* **4**, 389-417 (1986).

215   9.   M. E. Koshland, The coming of age of the immunoglobulin J chain. *Annu Rev Immunol*
216   **3**, 425-453 (1985).

217   10.   O. Pabst, New concepts in the generation and functions of IgA. *Nat Rev Immunol* **12**,
218   821-832 (2012).

219   11.   D. F. Robbiani *et al.*, Convergent antibody responses to SARS-CoV-2 in convalescent
220   individuals. *Nature*, (2020).

221   12.   F. Wu *et al.*, Evaluating the Association of Clinical Characteristics With Neutralizing
222   Antibody Levels in Patients Who Have Recovered From Mild COVID-19 in Shanghai,
223   China. *JAMA Intern Med*, (2020).

224   13.   B. Ju *et al.*, Human neutralizing antibodies elicited by SARS-CoV-2 infection. *Nature*,
225   (2020).

226   14.   P. J. M. Brouwer *et al.*, Potent neutralizing antibodies from COVID-19 patients define
227   multiple targets of vulnerability. *Science*, (2020).

228   15.   L. Liu *et al.*, Potent neutralizing antibodies directed to multiple epitopes on SARS-CoV-2

229   spike. *Nature*, (2020).

230   16.   Y. Wu *et al.*, A noncompeting pair of human neutralizing antibodies block COVID-19

231   virus binding to its receptor ACE2. *Science* **368**, 1274-1278 (2020).

232   17.   T. F. Rogers *et al.*, Isolation of potent SARS-CoV-2 neutralizing antibodies and

233   protection from disease in a small animal model. *Science*, (2020).

234   18.   S. J. Zost *et al.*, Potently neutralizing and protective human antibodies against SARS-

235   CoV-2. *Nature*, (2020).

236   19.   A. Baum *et al.*, REGN-COV2 antibody cocktail prevents and treats SARS-CoV-2

237   infection in rhesus macaques and hamsters. *bioRxiv*, 2020.2008.2002.233320 (2020).

238   20.   H. Ma *et al.*, Serum IgA, IgM, and IgG responses in COVID-19. *Cell Mol Immunol* **17**,

239   773-775 (2020).

240   21.   D. Sterlin *et al.*, IgA dominates the early neutralizing antibody response to SARS-CoV-2.

241   *medRxiv*, 2020.2006.2010.20126532 (2020).

242   22.   H. Q. Yu *et al.*, Distinct features of SARS-CoV-2-specific IgA response in COVID-19

243   patients. *Eur Respir J*, (2020).

244   23.   J. Seow *et al.*, Longitudinal evaluation and decline of antibody responses in SARS-CoV-

245   2 infection. *medRxiv*, 2020.2007.2009.20148429 (2020).

246   24.   X. Chi *et al.*, A neutralizing human antibody binds to the N-terminal domain of the Spike

247   protein of SARS-CoV-2. *Science*, (2020).

248   25.   Y. Cao *et al.*, Potent Neutralizing Antibodies against SARS-CoV-2 Identified by High-

249   Throughput Single-Cell Sequencing of Convalescent Patients' B Cells. *Cell* **182**, 73-84

250   e16 (2020).

251   26.   C. Kreer *et al.*, Longitudinal Isolation of Potent Near-Germline SARS-CoV-2-

252   Neutralizing Antibodies from COVID-19 Patients. *Cell*, (2020).

253   27.   F. Schmidt *et al.*, Measuring SARS-CoV-2 neutralizing antibody activity using

254   pseudotyped and chimeric viruses. *J Exp Med* **217**, (2020).

255   28.   R. Shi *et al.*, A human neutralizing antibody targets the receptor-binding site of SARS-

256   CoV-2. *Nature*, (2020).

257   29.   E. Seydoux *et al.*, Analysis of a SARS-CoV-2-Infected Individual Reveals Development

258   of Potent Neutralizing Antibodies with Limited Somatic Mutation. *Immunity* **53**, 98-105

259   e105 (2020).

260   30.   J. F. Scheid *et al.*, Broad diversity of neutralizing antibodies isolated from memory B

261   cells in HIV-infected individuals. *Nature* **458**, 636-640 (2009).

262   31.   Q. Wang *et al.*, A Combination of Human Broadly Neutralizing Antibodies against

263   Hepatitis B Virus HBsAg with Distinct Epitopes Suppresses Escape Mutations. *Cell Host*

264   *Microbe*, (2020).

265   32.   C. O. Barnes *et al.*, Structures of Human Antibodies Bound to SARS-CoV-2 Spike

266   Reveal Common Epitopes and Recurrent Features of Antibodies. *Cell*, (2020).

267   33.   M. Yuan *et al.*, Structural basis of a shared antibody response to SARS-CoV-2. *Science*,

268   (2020).

269   34.   M. Yuan *et al.*, A highly conserved cryptic epitope in the receptor binding domains of

270   SARS-CoV-2 and SARS-CoV. *Science* **368**, 630-633 (2020).

271   35.   S. A. Plotkin, Correlates of protection induced by vaccination. *Clin Vaccine Immunol* **17**,

272   1055-1065 (2010).

273   36.   K. Chen, G. Magri, E. K. Grasset, A. Cerutti, Rethinking mucosal antibody responses:

274   IgM, IgG and IgD join IgA. *Nat Rev Immunol* **20**, 427-441 (2020).

275   37.   A. Grifoni *et al.*, Targets of T Cell Responses to SARS-CoV-2 Coronavirus in Humans

276   with COVID-19 Disease and Unexposed Individuals. *Cell* **181**, 1489-1501 e1415 (2020).

277   38.   F. Amanat *et al.*, A serological assay to detect SARS-CoV-2 seroconversion in humans.

278   *Nat Med* **26**, 1033-1036 (2020).

279   39.   T. Tiller *et al.*, Efficient generation of monoclonal antibodies from single human B cells

280   by single cell RT-PCR and expression vector cloning. *J Immunol Methods* **329**, 112-124

281   (2008).

282   40.   L. von Boehmer *et al.*, Sequencing and cloning of antigen-specific antibodies from

283   mouse memory B cells. *Nat Protoc* **11**, 1908-1923 (2016).

284   41.   D. F. Robbiani *et al.*, Recurrent Potent Human Neutralizing Antibodies to Zika Virus in

285   Brazil and Mexico. *Cell* **169**, 597-609 e511 (2017).

286   42.   J. Ye, N. Ma, T. L. Madden, J. M. Ostell, IgBLAST: an immunoglobulin variable domain

287   sequence analysis tool. *Nucleic Acids Res* **41**, W34-40 (2013).

288   43.   N. T. Gupta *et al.*, Change-O: a toolkit for analyzing large-scale B cell immunoglobulin

289   repertoire sequencing data. *Bioinformatics* **31**, 3356-3358 (2015).

290   44.   C. Soto *et al.*, High frequency of shared clonotypes in human B cell receptor repertoires.

291   *Nature* **566**, 398-402 (2019).

292   45.   Y. Guo, K. Chen, P. D. Kwong, L. Shapiro, Z. Sheng, cAb-Rep: A Database of Curated

293   Antibody Repertoires for Exploring Antibody Diversity and Predicting Antibody

294   Prevalence. *Front Immunol* **10**, 2365 (2019).

295

Author contributions: Z.W., J.C.C.L., F.M., S.F. and M.C.N. conceived, designed and analyzed the experiments. Z.W., J.C.C.L., F.M., S.F., C.V., M.C., H.-H.H. L.N. and E.M. carried out all experiments. D.F.R., M. Caskey and C.G. designed clinical protocols. M.C., A.G. and D.O. produced antibodies. T.Y.O., and V.R. performed bioinformatic analysis. C.M.R., T.M. and P.D.B. helped designing the experiments. Z.W., J.C.C.L., F.M., S.F. and M.C.N. wrote the manuscript with input from all co-authors. **Declaration of conflict:** In connection with this work The Rockefeller University has filed a provisional patent application on which D.F.R. and M.C.N. are inventors. **Data and materials availability:** Data are provided in table S1, 2 ,4. The raw sequencing data associated with Fig. 3 has been deposited at Github (https://github.com/stratust/igpipeline). This study uses data from a database of human shared BCR clonotypes "https://cabrep.c2b2.columbia.edu/home/", and from 'cAb-Rep: A Database of

319   Curated Antibody Repertoires for Exploring Antibody Diversity and Predicting Antibody

320   Prevalence' and 'High frequency of shared clonotypes in human B cell receptor repertoires'.

321   Computer code to process the antibody sequences are available at GitHub

322   (https://github.com/stratust/igpipeline).

323
324   **Supplementary materials:**

325   Materials and Methods

326   Figs. S1 to S10

327   Tables S1 to S7

328   Reference (37-45)

329

330
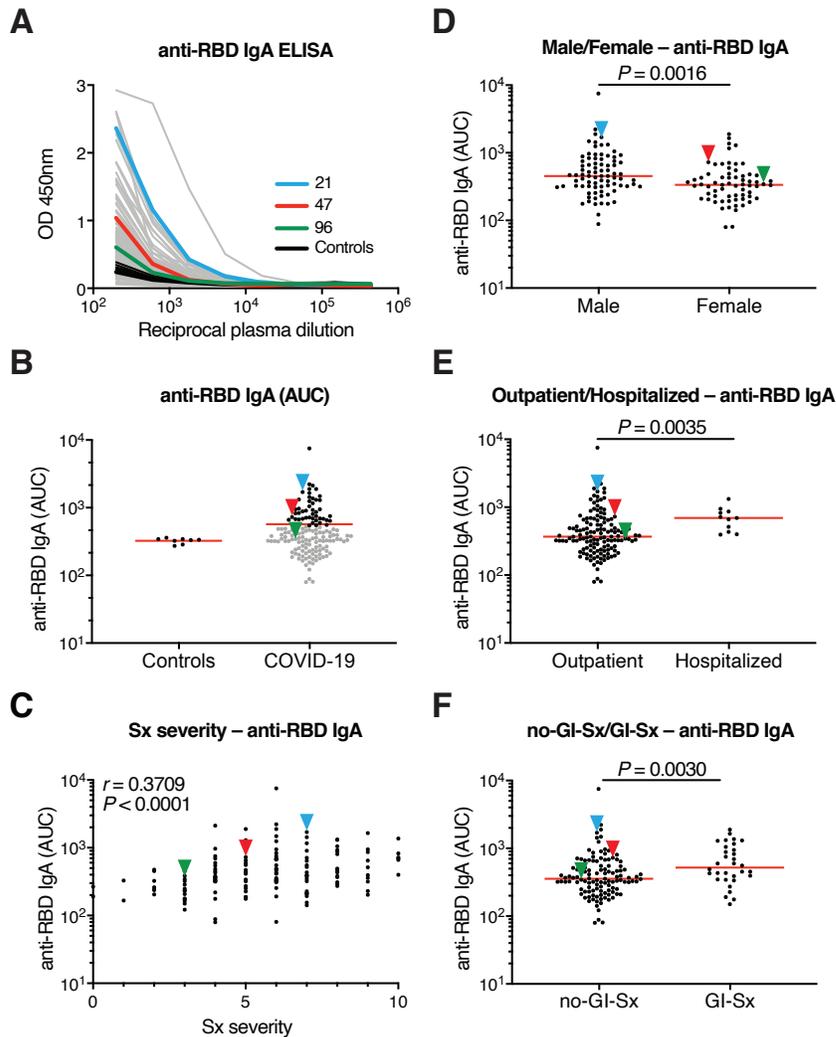
331
332 **Fig. 1 Plasma IgA against SARS-CoV-2 RBD.** (A) ELISAs measuring plasma IgA reactivity to

333 RBD. Graph shows optical density units at 450 nm (OD, Y axis) and reciprocal plasma dilutions

334 (X axis). Negative controls in black; individuals 21, 47, 96 in blue, red and green lines and

335 arrowheads, respectively (*11*). (B) Graph shows normalized area under the curve (AUC) for 8

336 controls and each of 149 individuals in the cohort. Horizontal bar indicates mean values. Black

337 dots indicate the individuals that are 2 STDV over the mean of controls. (C) Subjective Symptom

338 (Sx) severity (X axis) is plotted against the normalized AUC for IgA binding to RBD (Y axis). *r*

339      $= 0.3709$, $P < 0.0001$. (D) Normalized AUC of anti-RBD IgA ELISA for males (n=83) and

340   females (n=66); $P = 0.0016$. (E) Normalized AUC of anti-RBD IgA ELISA for outpatients

341   (n=138) and hospitalized (n=11) individuals; $P = 0.0035$. (F) Normalized AUC of anti-RBD IgA

342   ELISA for patients with gastrointestinal (GI) symptoms (n=32) and without GI symptoms

343   (n=117); $P = 0.0030$. The r and P values for the correlations in (C) were determined by two-

344   tailed Spearman's. For (D-F) horizontal bars indicate median values. Statistical significance was

345   determined using two-tailed Mann-Whitney U test.

346
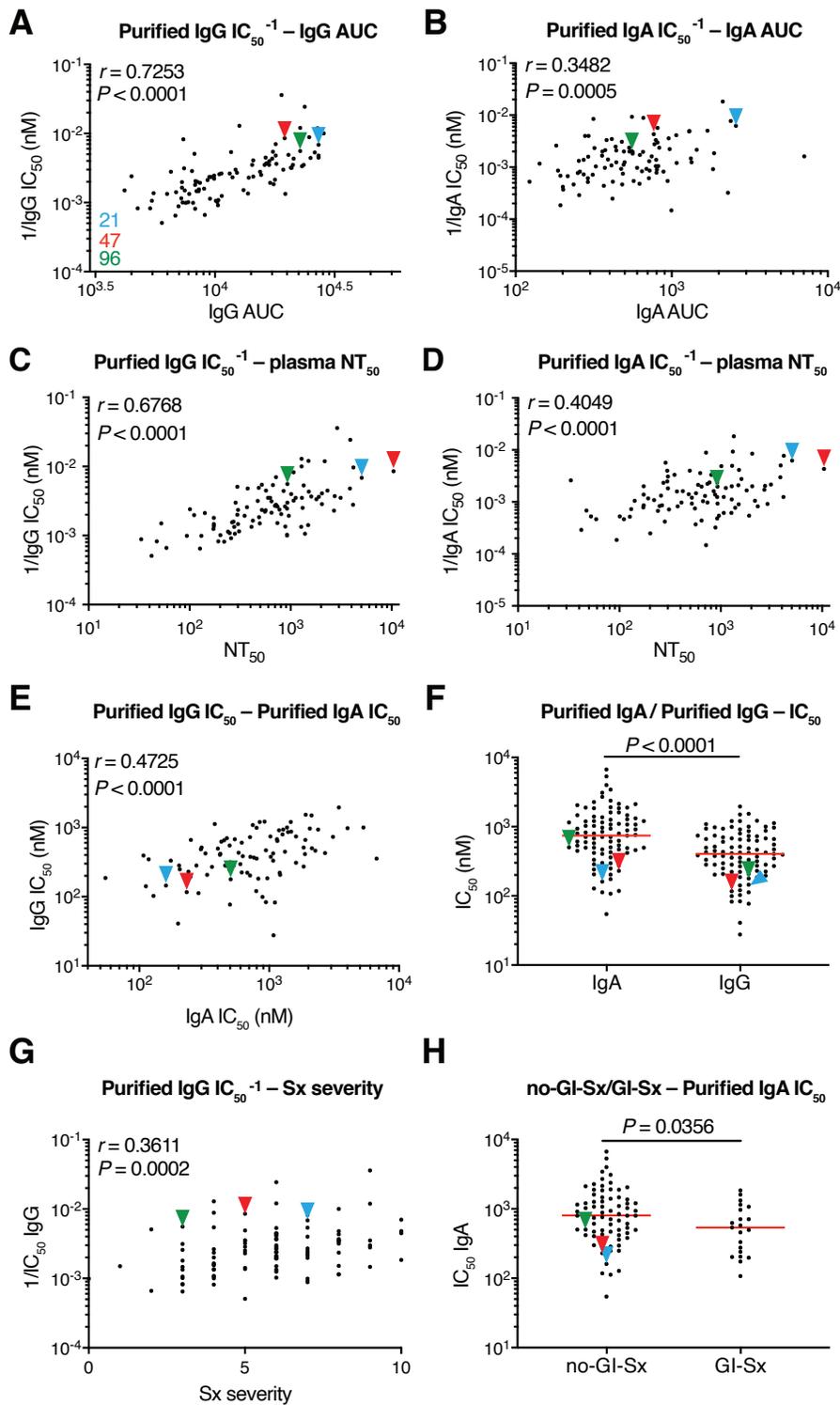
**Fig. 2 SARS-CoV-2 pseudovirus neutralization by purified IgA and IgG.** Neutralization

activity of plasma-purified IgG and IgA from 99 participants measured in cell lysates of

350   HT1080$_{ACE2}$cl.14 cells 48 h after infection with nanoluc-expressing SARS-CoV-2 pseudovirus.

351   (A) Normalized AUC for plasma IgG anti-RBD ELISA (X axis) plotted against purified IgG

352   pseudovirus neutralization $1/IC_{50}$ values (Y axis). $r = 0.7253$, $P < 0.0001$. (B) Normalized AUC

353   for plasma IgA ELISA (X axis) plotted against purified IgA pseudovirus neutralization $1/IC_{50}$

354   values (Y axis). $r = 0.3482$, $P = 0.0005$. (C) Published plasma NT_{50} values (*11*) (X axis) plotted

355   against purified IgG pseudovirus neutralization $1/IC_{50}$ values (Y axis). $r = 0.6768$, $P <$

356   0.0001. (D) Published plasma NT_{50} values (*11*) (X axis) plotted against purified IgA pseudovirus

357   neutralization $1/IC_{50}$ values (Y axis). $r = 0.4049$, $P < 0.0001$. (E) Purified IgA pseudovirus

358   neutralization IC_{50} values (X axis) plotted against purified IgG pseudovirus neutralization IC_{50}

359   values. $r = 0.4725$, $P < 0.0001$. (F) Comparison of purified IgA and IgG pseudovirus

360   neutralization IC_{50} values, $P < 0.0001$. (G) Symptom severity plotted against purified IgG

361   pseudovirus neutralization $1/IC_{50}$ values. $r = 0.3611$, $P = 0.0002$. (H) Purified IgA pseudovirus

362   neutralization IC_{50} values for patients with GI symptoms (n=21) and without GI symptoms

363   (n=74); $P = 0.0356$. The r and p values in (A-E, G) were determined by two-tailed Spearman's

364   correlations. In (F and H), p values were determined by two-tailed Mann–Whitney U-tests and

365   horizontal bars indicate median values.

366

367

368
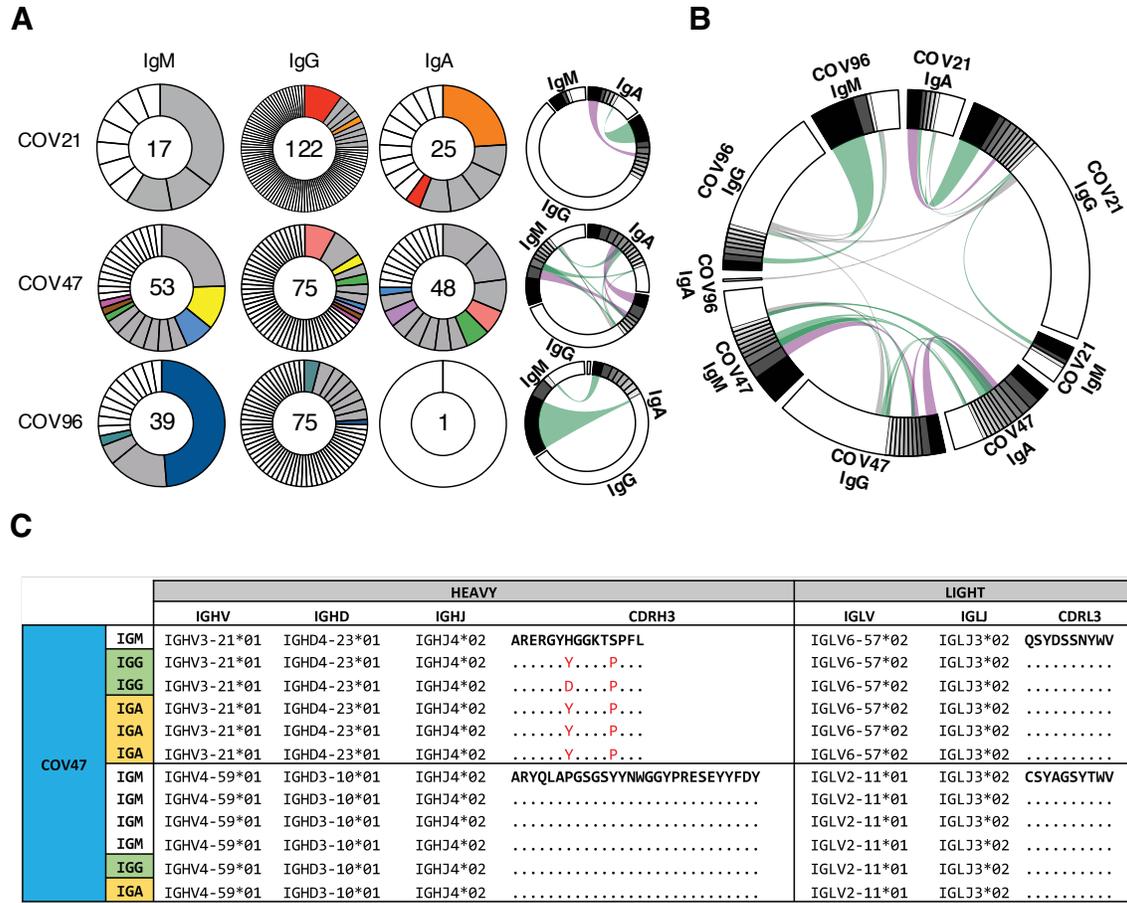
Fig. 3 Monoclonal anti-SARS-CoV-2 RBD IgM, IgG and IgA. (A) Clonal expansion of B cells producing of IgM, IgG and IgA from three individuals. The number in the inner circle indicates the number of sequences analyzed for the individual denoted above the circle. Pie slices size is proportional to the number of clonally related sequences. Colored pie slices indicate clones or singlets that share the same IGHV and IGLV genes, and highly similar CDR3s. Grey indicates clones that are not shared. White indicates singlets that are not shared. The right side circos plots show the relationship between antibodies of different isotypes that share same IGH V(D)J and IGL VJ genes, and highly similar CDR3s. Purple, green and grey lines connect related

378   clones, clones and singles, and singles to each other, respectively. (B) Circos plot shows

379   sequences from all 3 individuals with clonal relationships depicted as in (A). (C) Sample

380   sequence alignment for antibodies of different isotypes that display same IGH V(D)J and IGL VJ

381   genes and highly similar CDR3s. Amino acid differences in CDR3s to the reference sequence

382   (bold) are indicated in red, dashes indicate missing amino acids and dots represent identical

383   amino acids.

384

385

386
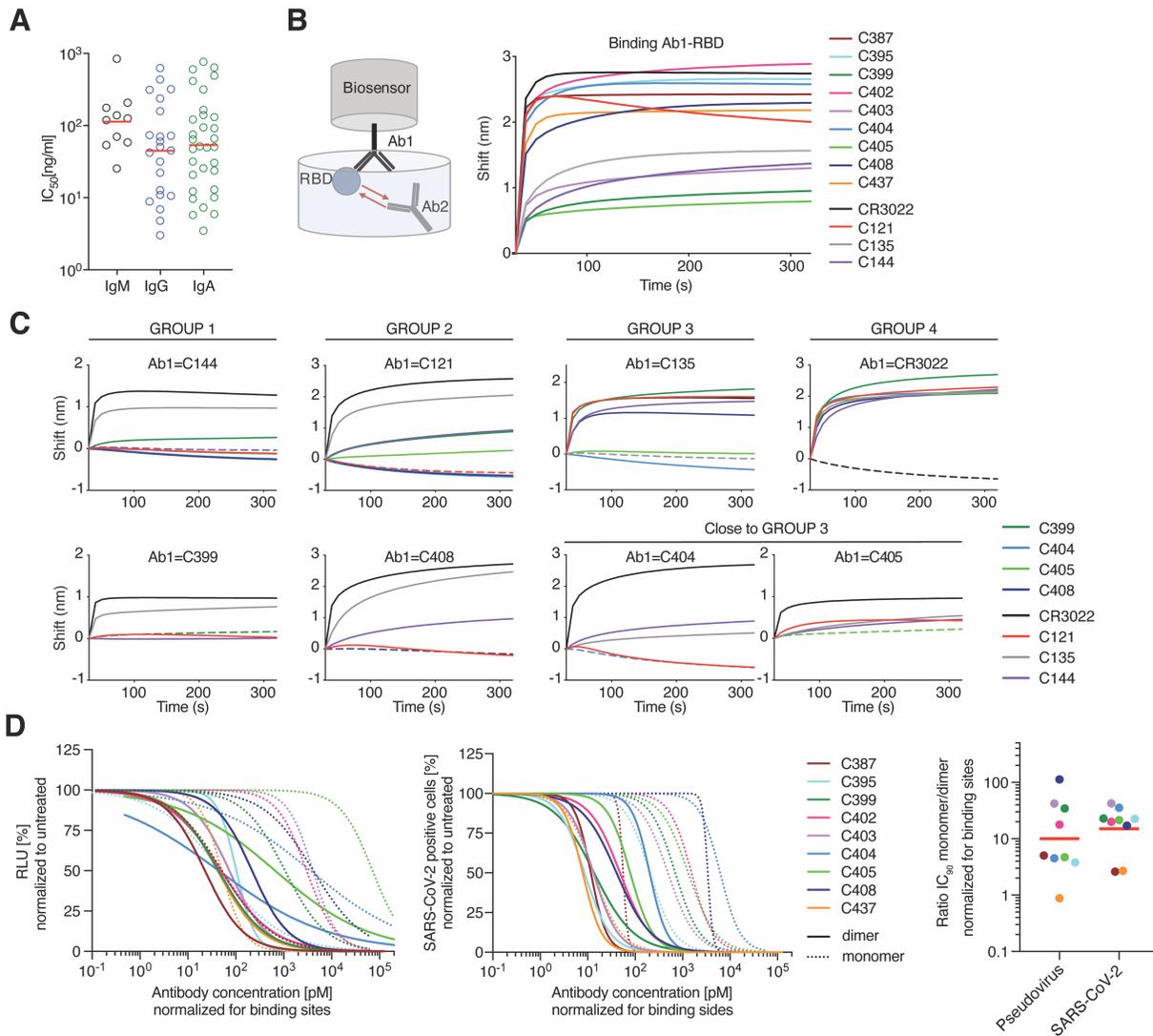
Fig. 4 IgA dimers neutralize SARS-CoV-2 more potently than monomers. (A) Pseudovirus IC$_{50}$ neutralization values for IgA, and IgM monoclonals and published IgG monoclonals from the same individuals (*11*). Antibodies with IC$_{50}$ less than 1000 ng/ml are shown. Red lines indicate geometric mean. (B) Diagrammatic representation of biolayer interferometry experiment (left panel). Binding of C387, C395, C399, C402, C403, C404, C405, C408, C437, CR3022, C121, C135, C144 to RBD (right panel). (C) Second antibody (Ab2) binding to preformed first antibody (Ab1)–RBD complexes. Dotted line denotes when Ab1 and Ab2 are the same, and Ab2

394   is according to the colour-coding in g. h, l, Group 1 antibodies were tested. (D) The normalized

395   relative luminescence values for cell lysates of $293T_{ACE2}$ cells after infection with SARS-CoV-2

396   pseudovirus (left panel) or normalized percentage of SARS-CoV-2 positive VeroE6 cells 48 h

397   after infection with SARS-CoV-2 authentic virus (middle panel; values obtained in the absence

398   of antibody are plotted at x=0.1 to be visible on log-scale) in the presence of increasing

399   concentrations of monoclonal antibodies C387, C395, C399, C402, C403, C404, C405, C408,

400   C437 as monomers or dimers. Shown are four-parameter nonlinear regression curve fits of

401   normalized data. Comparison of the ratio of IC_{90} values of monomer to dimers, normalized to

402   number of antibody binding sites (right panel).

403

404 **Materials and Methods**

405 **Human Study participants**

406 Samples were obtained from 149 individuals under a study protocol approved by the Rockefeller University in New

407 York from April 1 through May 8, 2020 as described in (*11*). All participants provided written informed consent

408 before participation in the study and the study was conducted in accordance with Good Clinical Practice and clinical

409 data collection. The study was performed in compliance with all relevant ethical regulations and the protocol was

410 approved by the Institutional Review Board (IRB) of the Rockefeller University.

411

412 **Purification and quantification of IgA and IgG from plasma**

413 IgA and IgG were purified from samples with measurable neutralizing activity, against SARS-CoV-2-RBD (*11*).

414 300μl of plasma was diluted with PBS heat-inactivated (56°C for 1 hr) and incubated with peptide M/Agarose

415 (Invivogen) or Protein G/Agarose (GE lifeSciences) overnight at 4 °C. The suspension was transferred to

416 chromatography columns and washed with 10 column volumes of 1X-PBS. IgA and IgG were then eluted with

417 1.5ml of 0.1M glycine (pH=3.0) and pH was immediately adjusted to 7.5 with 1M Tris (pH=8.0). 1X-PBS buffer

418 exchange was achieved using Amicon® Ultra centrifugal filters (Merck Millipore) through a 30-kD membrane

419 according to the manufacturer's instructions. IgA and IgG concentrations were determined by measurement of

420 absorbance at 280nm using a NanoDrop (Thermo Scientific) instrument and samples were stored at 4°C.

421

422 **ELISAs**

423 ELISAs to evaluate the IgG or IgA binding to SARS-CoV-2 RBD were performed as previously described using a

424 validated assay (*37, 38*). High binding 96 half well plates (Corning #3690) were coated with 50 μL per well of a

425 1μg/mL protein solution in PBS overnight at 4 °C. Plates were washed 6 times with washing buffer (1xPBS with

426 0.05% Tween 20 (Sigma-Aldrich)) and incubated with 170 μL blocking buffer per well (1xPBS with 2% BSA and

427 0.05% Tween20 (Sigma) for 1 hour at room temperature (RT). Immediately after blocking, monoclonal antibodies

428 or plasma samples were added in PBS and incubated for 1 hr at RT. Plasma samples were assayed at a 1:200 starting

429 dilution and seven additional 3-fold serial dilutions. Monoclonal antibodies were tested at 10 μg/ml starting

430 concentration and 10 additional 4-fold serial dilutions. Plates were washed 6 times with washing buffer and then

431 incubated with anti-human IgG (Jackson Immuno Research 109-036-088) or anti-human IgA (Sigma A0295)

432 secondary antibody conjugated to horseradish peroxidase (HRP) in blocking buffer at 1:5000 or 1:3000 dilution

433 respectively. Plates were developed by addition of the HRP substrate, TMB (ThermoFisher) for 10 minutes (plasma

434 samples) or 4 minutes (monoclonal antibodies), then the developing reaction was stopped by adding 50µl 1M

435 H_2SO_4. ODs were measured at 450 nm in a microplate reader (FluoStar Omega, BMG Labtech). For plasma

436 samples, a positive control (plasma from patient COV21, diluted 200-fold in PBS) and negative control historical

437 plasma samples was added in duplicate to every assay plate for validation. The average of its signal was used for

438 normalization of all the other values on the same plate with Excel software prior to calculating the area under the

439 curve using Prism 8 (GraphPad).

440

441 **Cell lines**

442 HT1080$_{Ace2}$ cl.14 cells (*27*), 293T$_{Ace2}$ cells (*11*) and VeroE6 kidney epithelial cells were cultured in Dulbecco's

443 modified Eagle medium (DMEM) supplemented with 10% FCS at 37 °C and 5% CO_2. In addition, medium for

444 Ace2-overexpressing cell lines contained 5 µg/ml blasticidin and medium for VeroE6 cells was supplemented with 1

445 % nonessential amino acids. All cell lines have been tested negative for contamination with mycoplasma and

446 parental cell lines were obtained from the ATCC.

447

448 **Pseudotyped virus neutralization assay**

449 SARS-CoV-2 pseudotyped particles were produced by co-transfection of pSARS-CoV-2 S$_{trunc}$ and pNL4-3ΔEnv-

450 nanoluc in 293T cells (*11, 27*). Four-fold serially diluted purified plasma IgG/IgA from COVID-19 convalescent

451 individuals and healthy donors or monoclonal antibodies were incubated with the SARS-CoV-2 pseudotyped virus

452 for 1 hour at 37 °C. Subsequently, the mixture was incubated with Ace2-expressing cells for 48 hours. HT1080$_{Ace2}$

453 cl. 14 cells (*27*) were used for plasma-derived IgG/IgA and 293T$_{Ace2}$ cells (*11*) for monoclonal antibodies. Following

454 incubation, cells were washed twice with PBS and lysed with Luciferase Cell Culture Lysis 5x reagent (Promega).

455 Nanoluc Luciferase activity in lysates was measured using the Nano-Glo Luciferase Assay System (Promega) with a

456 GloMax Natigator Microplate Luminometer (Promega). Relative luminescence units obtained were normalized to

457 those derived from cells infected with SARS-CoV-2 pseudotyped virus in the absence of plasma-derived or

458 monoclonal antibodies. The half-maximal and 90% inhibitory concentrations for purified plasma IgG or IgA or

459 monoclonal antibodies (IC50 and IC90) were determined using 4-parameter nonlinear regression (GraphPad Prism).

460

461

462 **Antibody sequencing, cloning and expression**

463 Single B cells were isolated from COV21, COV47 and COV96 patients as previously described(*11*). Briefly, RNA

464 from single cells was reverse-transcribed (SuperScript III Reverse Transcriptase, Invitrogen, 18080-044) using

465 random primers (Invitrogen, 48190011) and followed by nested PCR amplifications and sequencing using the

466 primers for heavy chain that are listed in (table S7) and primers light chains from (*39*). Sequence analysis was

467 performed with MacVector. Antibody cloning from PCR products was performed as previously described by

468 sequencing and ligation-independent cloning into antibody expression vectors (Igγ1-, IGκ-, IGλ-, Igα1 and Igα2) as

469 detailed in (*40*). The Igα1 and Igα2 vectors were from (Invivogen, pfusess-hcha1for IgA1 and pfusess-hcha2m1 for

470 IgA2). J chain plasmid was a gift from Susan Zolla-Pazner. Recombinant monoclonal antibodies were produced and

471 purified as previously described (*39, 41*). Briefly, monoclonal antibodies were produced by transient co-transfection

472 of 293-F cells with human heavy chain and light chain antibody expression plasmids using polyethylenimine (PEI)

473 (Sigma-Aldrich, catalog #408727). Seven days after transfection, supernatants were harvested, clarified by

474 centrifugation and subsequently incubated with Peptide M(Invivogen)/Protein G-coupled sepharose beads

475 (Invivogen, catalog# gel-pdm-5; GE healthcare, 17-0618-05) overnight at 4°C. For dimers, antibodies were

476 produced by transient transfection of Expi293F cells with heavy chain, light chain and J chain expression plasmids

477 at a 1:1:1 ratio. After five days, antibodies were harvested, filtered, incubated with Peptide M overnight and eluted.

478

479 **Separation of Dimeric IgA from its Monomeric Form by Size Exclusion Chromatography**

480 A Pre-packed HiLoad™ 16/60 Superdex™ 200 pg (Cytiva, catalog #28989335) on the NGC™ Quest 10 Plus

481 Chromatography System by Bio-Rad was calibrated at room temperature using the HMW Gel Filtration Calibration

482 Kit (Cytiva, catalog #28403842) and IgG. After equilibration of the column with PBS, each concentrated IgA

483 preparation was applied onto the column using a 1 ml-loop at a flow rate of 0.5 ml/min. Dimers of IgA1 or IgA2

484 were separated from monomers upon an isocratic elution with 70 ml of PBS. The fractions were pooled,

485 concentrated and evaluated by SDS-PAGE using 4 –12% Bis–Tris Novex gels (GenScript catalog #M00652) under

486 reducing and non-reducing conditions followed by a Coomassie blue staining (Expedeon, catalog #ISB1L).

487

Microneutralization assay with authentic SARS-CoV-2.

Production of SARS-CoV-2 virus was performed as previously described (*11*). This assay was performed as described previously (*11, 42*). VeroE6 cells were seeded at $1x10^4$ cells/well into 96-well plates on the day before infection. IgA monomers and dimers were serially diluted (4-fold) in BA-1, consisting of medium 199 (Lonza, Inc.) supplemented with 1% bovine serum albumin (BSA) and 1x penicillin/streptomycin. The diluted samples were mixed with a constant amount of SARS-CoV-2 and incubated for 1hr at 37°C. The antibody-virus-mix was then directly applied to VeroE6 cells (MOI of ~0.1 PFU/cell; n=3) and incubated for 22h at 37°C. Cells were subsequently fixed by adding an equal volume of 7% formaldehyde to the wells, followed by permeabilization with 0.1% Triton X-100 for 10 min. After extensive washing, cells were incubated for 1hr at 37°C with blocking solution of 5% goat serum in PBS (catalog no. 005–000-121; Jackson ImmunoResearch). A rabbit polyclonal anti-SARS-CoV-2 nucleocapsid antibody (catalog no. GTX135357; GeneTex) was added to the cells at 1:1,000 dilution in blocking solution and incubated at 4 °C overnight. Goat anti-rabbit AlexaFluor 594 (catalog no. A-11012; Life Technologies) was used as a secondary antibody at a dilution of 1:2,000. Nuclei were stained with Hoechst 33342 (catalog no. 62249; Thermo Scientific) at a 1:1,000 dilution. Images were acquired with a fluorescence microscope and analyzed using ImageXpress Micro XLS (Molecular Devices, Sunnyvale, CA). All experiments involving SARS-CoV-2 were performed in a biosafety level 3 laboratory.

Biolayer interferometry

BLI assays were performed on the Octet Red instrument (ForteBio) at 30 °C with shaking at 1,000 r.p.m. Epitope binding assays were performed with protein A biosensor (ForteBio 18-5010), following the manufacturer's protocol "classical sandwich assay". (1) Sensor check: sensors immersed 30 sec in buffer alone (buffer ForteBio 18-1105). (2) Capture 1st Ab: sensors immersed 10 min with Ab1 at 40 μg/mL. (3) Baseline: sensors immersed 30 sec in buffer alone. (4) Blocking: sensors immersed 5 min with IgG isotype control at 50 μg/mL. (6) Antigen association: sensors immersed 5 min with RBD at 100 μg/mL. (7) Baseline: sensors immersed 30 sec in buffer alone. (8) Association Ab2: sensors immersed 5 min with Ab2 at 40 μg/mL. Curve fitting was performed using the Fortebio Octet Data analysis software (ForteBio).

Computational analyses of antibody sequences

516 Antibody sequences were trimmed based on quality and annotated using Igblastn v1.14.0[ref] with IMGT domain

517 delineation system. Annotation was performed systematically using Change-O toolkit v.0.4.5(*43*). Heavy and light

518 chains derived from the same cell were paired, and clonotypes were assigned based on their V and J genes using in-

519 house R and Perl scripts (Fig. 3 A and B). All scripts and the data used to process antibody sequences are publicly

520 available on GitHub (https://github.com/stratust/igpipeline). Nucleotide somatic hypermutation and CDR3 length

521 were determined using in-house R and Perl scripts. For somatic hypermutations, IGHV and IGLV nucleotide

522 sequences were aligned against their closest germlines using Igblastn and the number of differences were considered

523 nucleotide mutations. The average mutations for V genes was calculated by dividing the sum of all nucleotide

524 mutations across all patients by the number of sequences used for the analysis. Hydrophobicity distribution

525 comparisons were calculated as described in (*11*) (Fig. S5). The frequency distributions of human V genes in anti-

526 SARS-CoV-2 antibodies from this study was compared to 131,284,220 IgH and IgL sequences generated by (*44*)

527 and downloaded from cAb-Rep (*45*), a database of human shared BCR clonotypes available at https://cab-

528 rep.c2b2.columbia.edu/. Based on the 81 distinct V genes that make up the 1455 analyzed sequences from Ig

529 repertoire of the three patients present in this study, we selected the IgH and IgL sequences from the database that

530 are partially coded by the same V genes and counted them according to the constant region. The frequencies shown

531 in (Fig. S6) are relative to the source and isotype analyzed. We used the two-sided binomial test to check whether

532 the number of sequences belonging to a specific IgHV or IgLV gene in the repertoire is different according to the

533 frequency of the same IgV gene in the database. Adjusted p-values were calculated using the false discovery rate

534 (FDR) correction. Significant differences are denoted with stars.

535

536

537
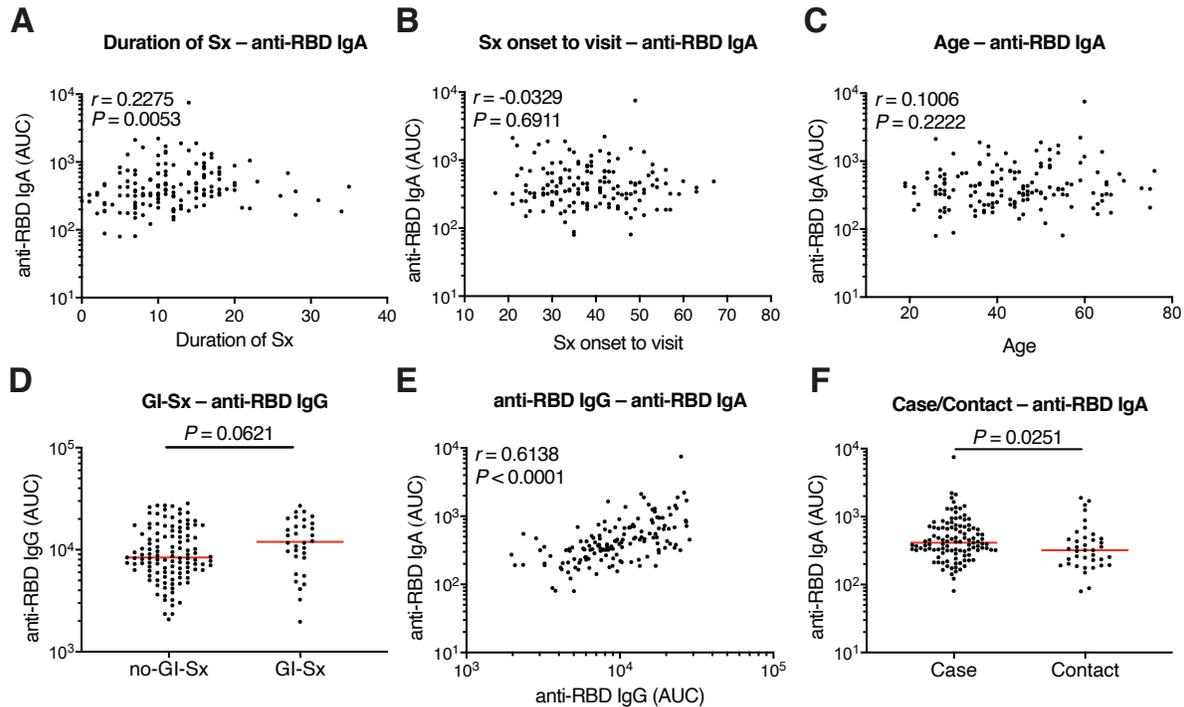
Fig. S1 Clinical correlates of plasma IgA antibody titers (A) Duration of Symptom (Sx) in days (X axis) plotted

against normalized AUC for plasma IgA binding to RBD (Y axis). $r = 0.2275$, $P = 0.0053$. (B) Sx onset to time of

sample collection in days plotted against normalized AUC for plasma IgA anti-RBD. $r = -0.0329$ and $P = 0.6911$.

(C) Age plotted against normalized AUC for plasma IgA anti-RBD. $r = 0.1006$, $P = 0.2222$. (D) Normalized AUC

of plasma anti-RBD IgG ELISA for patients with gastrointestinal (GI) symptoms (n=32) and without GI symptoms

(n=117); $P = 0.0621$. (E) Normalized AUC of plasma anti-RBD IgG ELISA plotted against normalized AUC for

plasma IgA anti-RBD. $r=0.6138$, $P < 0.0001$. (F) Normalized AUC of plasma anti-RBD IgA ELISA for all cases (n

= 111) and contacts (n = 38) in the cohort; $P = 0.0251$. For (A-C, E) the correlations were analyzed by two-tailed

Spearman's tests; For (D and F), Horizontal bars indicate median values. Statistical significance was determined

using two-tailed Mann–Whitney U-tests.

548
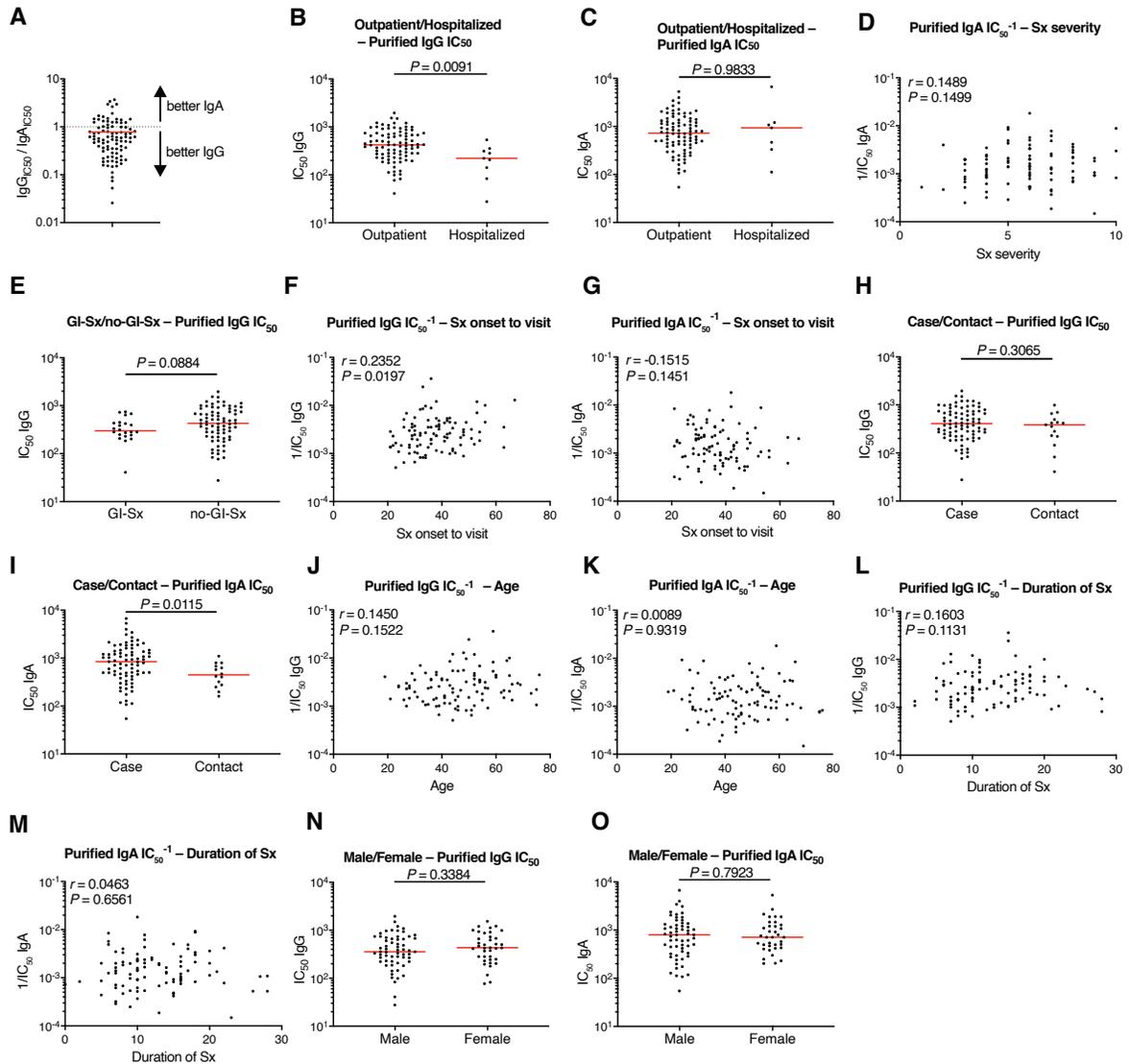
Fig. S2 Clinical correlates of plasma IgA/IgG neutralization (A) Ratio of pseudovirus neutralization IC_{50} values of purified IgG to IgA (n=95). (B, C) Purified plasma IgG (B) and IgA(C) pseudovirus neutralizing IC_{50} values for all outpatient (n = 90) and hospitalized (n = 9) participants in the cohort. (Fig. S2B, $P = 0.0091$) and (Fig. S2C, $P = 0.9833$). (D) Purified plasma IgA $1/IC_{50}$ values plotted against symptom severity. $r = 0.1489$, $P=0.1499$. (E) Purified plasma IgG IC_{50} values for patients with GI symptoms (n=22) and without GI symptoms (n=77); $p=0.0884$. (F, G) Sx onset to time of sample collection in days plotted against purified plasma IgG (F) and IgA(G) pseudovirus neutralization $1/IC_{50}$ values. (Fig. S2F, $r = 0.2352$, $P = 0.0197$) and (Fig. S2G, $r = -0.1515$, $P = 0.1451$). (H, I) Purified plasma IgG (H) and IgA(I) pseudovirus neutralization IC_{50} values for all cases (n = 84) and contacts (n = 15) in the cohort. (Fig. S2H, $P = 0.3065$) and (Fig. S2I, $P = 0.0115$). (J, K) Age plotted against purified plasma IgG

30

558   (J) and IgA(K) pseudovirus neutralization $1/IC_{50}$ values. (Fig. S2J, $r = 0.1450$, $P = 0.1522$) and (Fig. S2K, $r =$

559   0.0089, $P = 0.9319$). (L, M) Duration of Symptom (Sx) in days (X axis) plotted against purified plasma IgG (L) and

560   IgA(M) pseudovirus neutralization $1/IC_{50}$ values. (Fig. S2L, $r = 0.1603$, $P = 0.1131$) and (Fig. S2M, $r = 0.0463$, $P =$

561   0.6561). (N, O) Purified plasma IgG (N) and IgA(O) pseudovirus neutralization IC_{50} values for males (n=61) and

562   females (n=38). (Fig. S2N, $P=0.3384$) and (Fig.S2O, $P=0.7923$). For (A), horizontal bars indicate mean value. For

563   (B, C, E, H, I, N, O), horizontal bars indicate median values. Statistical significance was determined using two-tailed

564   Mann–Whitney U-tests; For (D, F, G, J-M), the correlations were analyzed by two-tailed Spearman's tests.

565
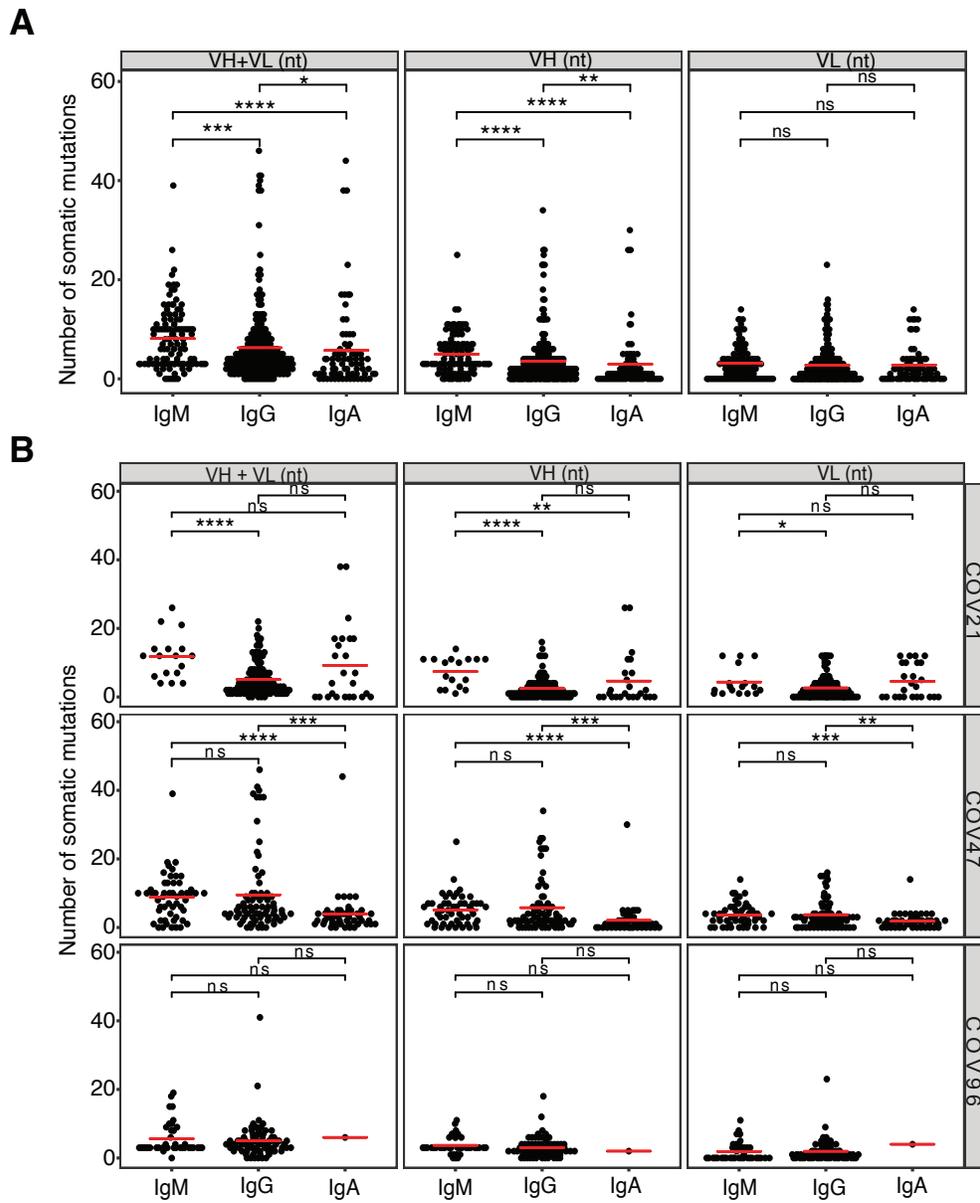
Fig. S3 Analysis of antibody somatic hypermutation

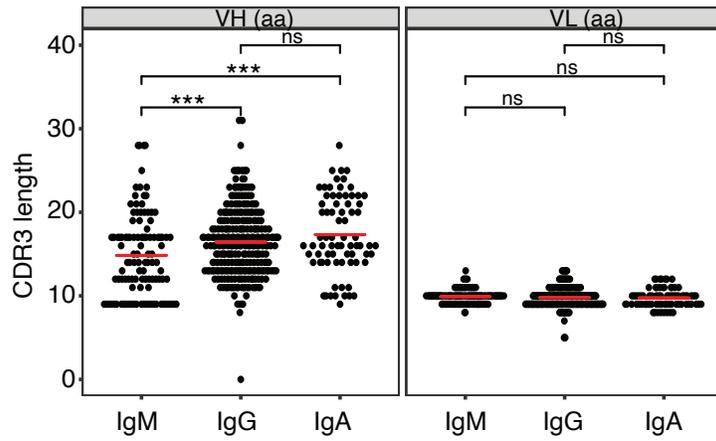(A) The number of somatic nucleotide mutations (Y axis) at the IGVH and IGVL for IgM, IgG and IgA antibodies (X axis), the horizontal bars indicate the mean. The number of antibody sequences was evaluated for both IGVH and IGVL. (n=455). (B) Same as (A) but for each individual.
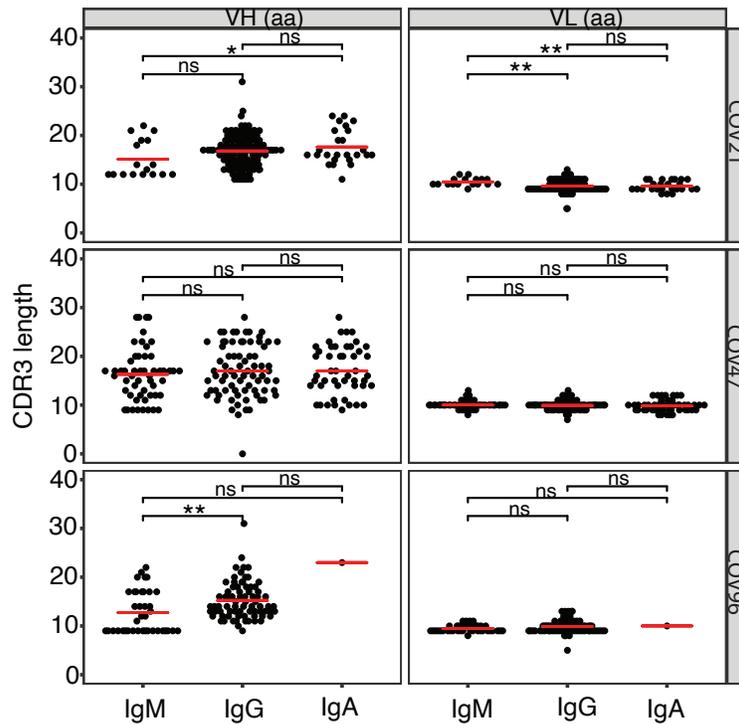
A

B
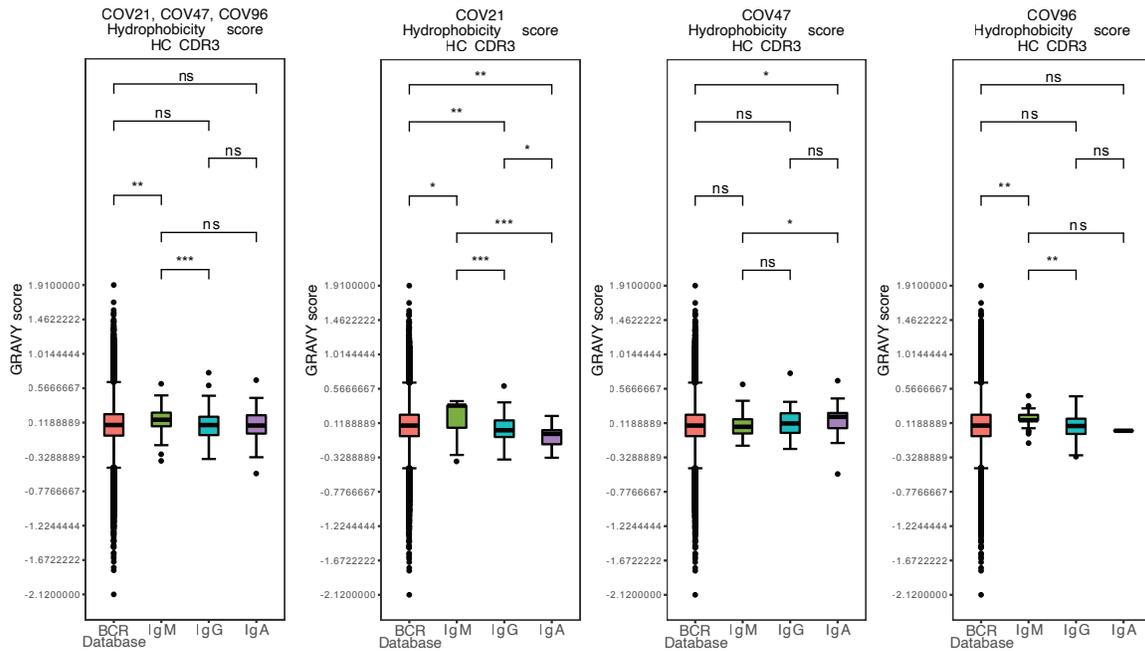

Fig. S4 Analysis of antibody CDR3 length

(A) IGVH and IGVL CDR3s length (Y axis) for IgM, IgG and IgA (X axis). (B) Same as (A) but for each

individual. The horizontal bars indicate the mean.

576

577

Fig. S5 Analysis of antibody CDR3 hydrophobicity

Distribution of the hydrophobicity GRAVY scores at the IGH CDR3 in antibody sequences from this study

compared to a public database (see Methods for statistical analysis). The box limits are at the lower and upper

quartiles, the center line indicates the median, the whiskers are 1.5x interquartile range and the dots represent

outliers.

583
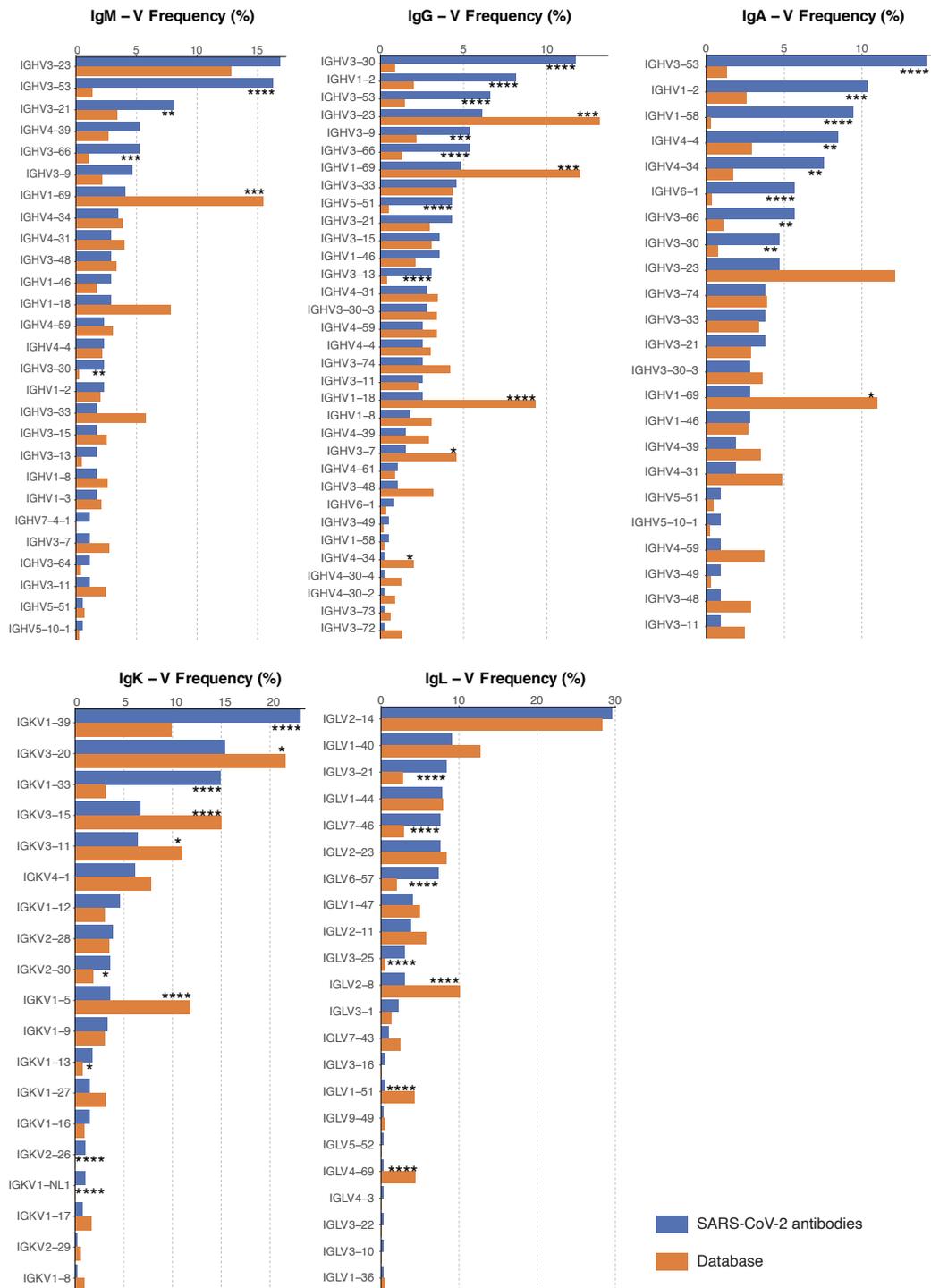
Fig. S6 Frequency distributions of human V genes.

Comparison of the frequency distributions of human V genes for heavy chain (IgM, IgG and IgA) and light chains of anti-SARS-CoV-2 antibodies from this study and from a database of shared clonotypes of human B cell receptor

588   generated by Cinque Soto et al. (*44*). Statistical significance was determined using the two-sided binomial test.

589   Significant differences are denoted with stars.

590

591

592
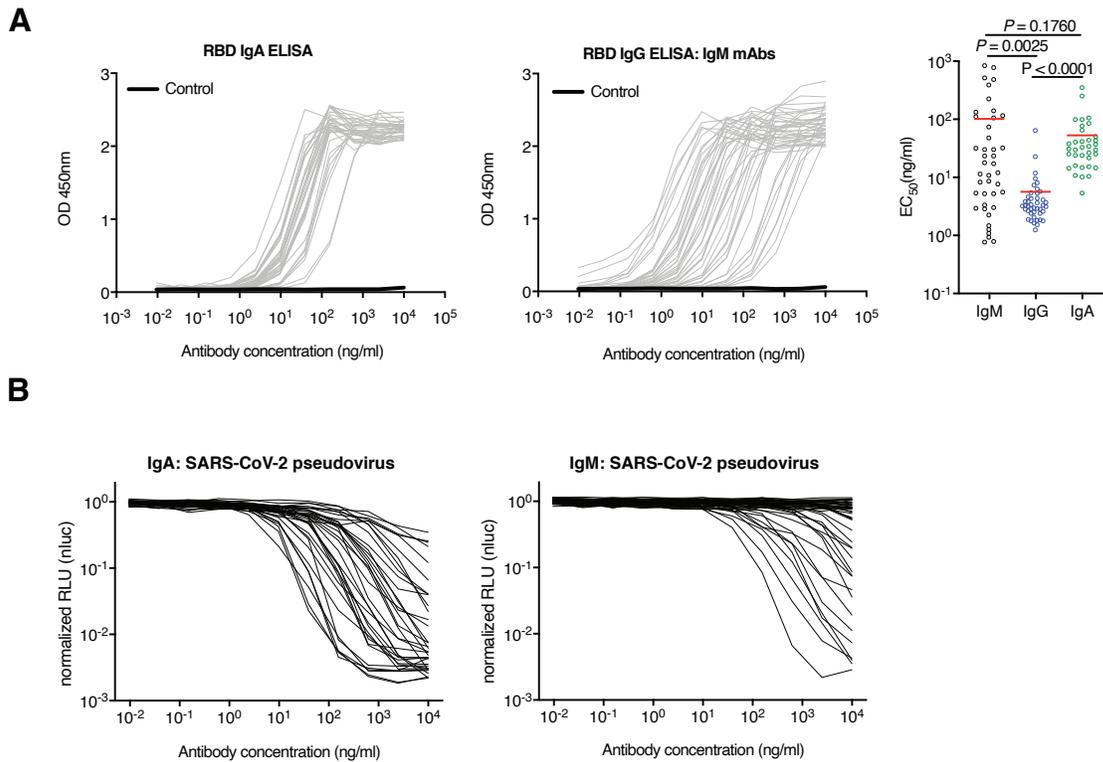
Fig. S7 Binding and neutralizing activity of anti-SARS-CoV-2 RBD IgA and IgM monomers.

(A) Binding profiles of 35 IgA and 46 IgM monoclonals against RBD. Comparisons of IgM, published IgG (*11*) and

IgA EC_{50} values shown as in right panel. Red lines indicate mean value. (B) The normalized relative luminescence

values for cell lysates of $293T_{ACE2}$ cells 48 h after infection with SARS-CoV-2 pseudovirus in the presence of

increasing concentrations of monoclonal IgA and IgM antibodies. Statistical analysis was performed using the

student's *t* test.

599

A

B
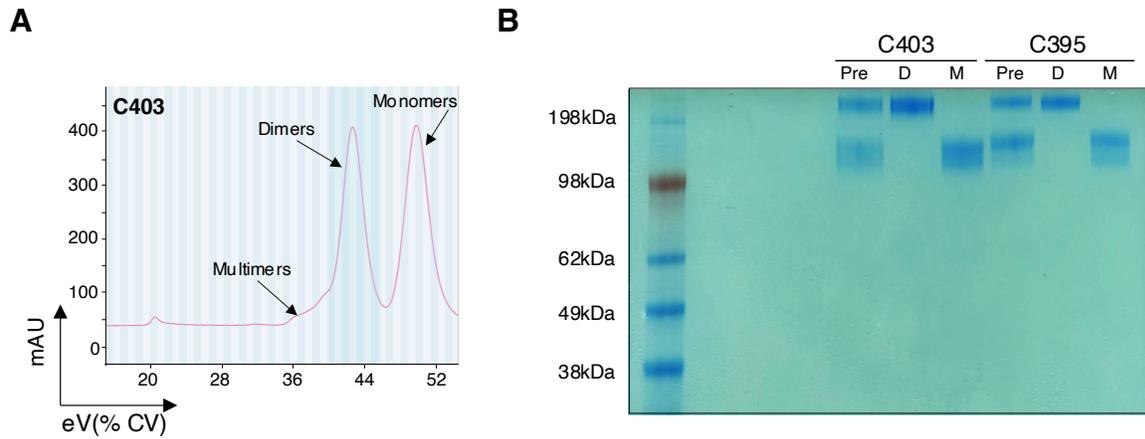
Fig. S8 Purification of Dimeric IgA by Size Exclusion Chromatography. (A) Monomers and dimers of IgA1 or IgA2 were separated using a Superdex 200 (Cytiva) with PBS at a flow rate of 0.5 ml/min. Representative example: C403. The X axis is elution volume (eV) as a percent of Column volume. The Y axis is absorption at 280nm (mAU). (B) Coomassie Blue stained non-reducing SDS-PAGE gel of pre-separation antibody mixture (Pre), isolated dimers (D) and monomers (M).

607
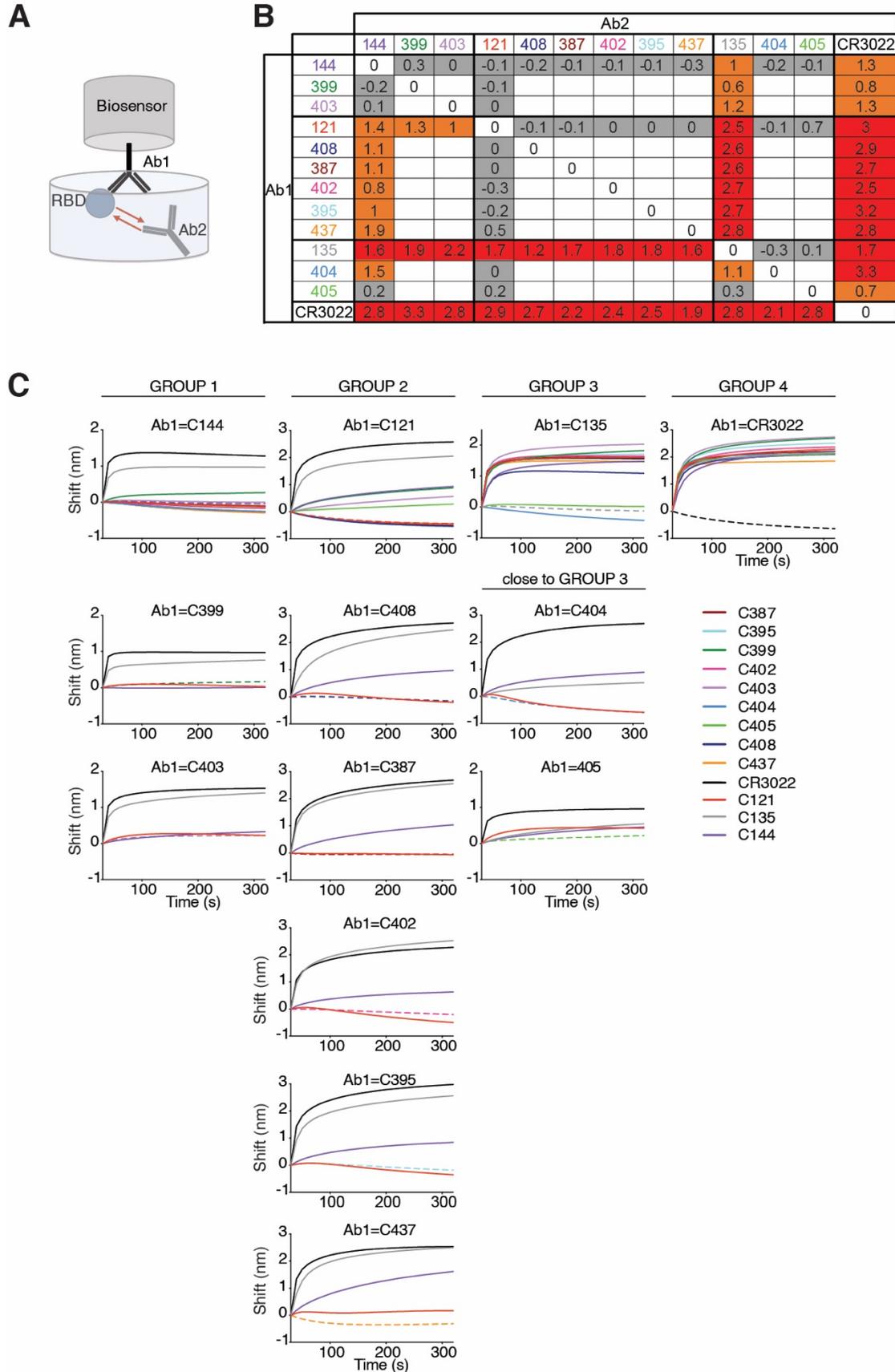
608 **Fig. S9 Biolayer interferometry experiment.** (A) Diagrammatic representation of biolayer interferometry

609 experiment. (B) The table displays the shift in nanometers after second antibody (Ab2) binding to the antigen in the

610 presence of the first antibody (Ab1). Values are normalized by the subtraction of the autologous antibody control.

611 (C) Second antibody (Ab2) binding to preformed first antibody (Ab1)–RBD complexes. Dotted line denotes when

612 Ab1 and Ab2 are the same, and Ab2 is according to the colour-coding in Fig. 4B (right panel).

613

614
615

616
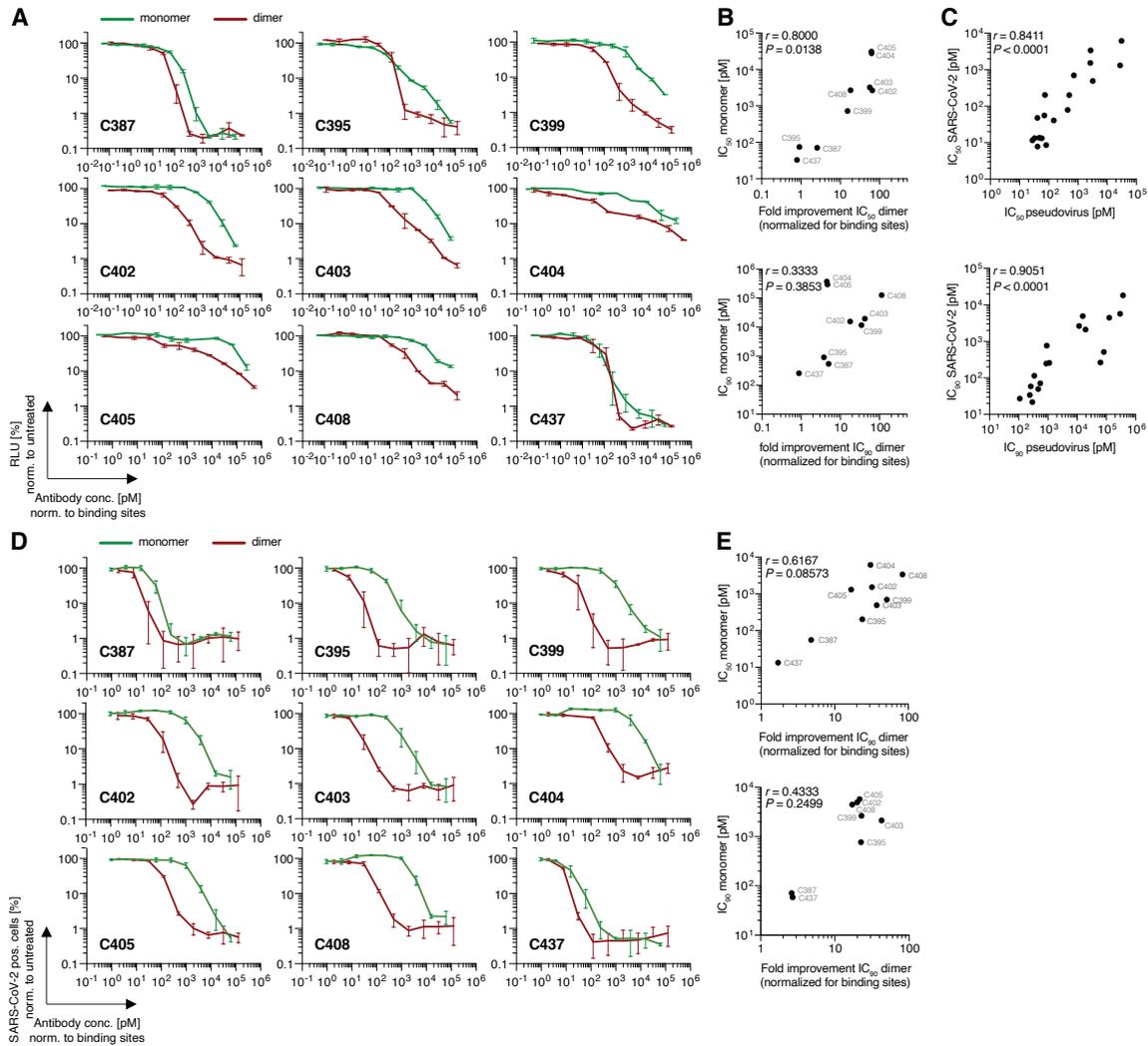
Fig. S10 Neutralizing activity of monoclonal monomeric and dimeric IgAs

(A) The normalized relative luminescence values for cell lysates of $293T_{ACE2}$ cells 48 h after infection with SARS-CoV-2 pseudovirus in the presence of increasing concentrations of monoclonal antibodies C387, C395, C399, C402, C403, C404, C405, C408, C437 in their monomeric (green curves) and dimeric (red curves) form. (B) Fold improvement of the IC_{50} (upper panel) and IC_{90} (lower panel) values of dimeric IgA to monomeric IgA (X axis) plotted against IC_{50} ($r = 0.8000$, $P = 0.0138$), IC_{90} ($r = 0.3333$, $P = 0.3853$) values of monomeric IgAs. (C) IC_{50} (upper panel) and IC_{90} (lower panel) values of dimeric and monomeric IgAs determined by pseudovirus neutralization assay (x axis) plotted against IC_{50} ($r = 0.8411$, $P < 0.0001$) and IC_{90} ($r = 0.9051$, $P < 0.0001$) values

625   determined by authentic SARS-CoV-2 neutralization assay (y axis). (D) SARS-CoV-2 neutralization assay. The

626   normalized percentage of SARS-CoV-2 positive VeroE6 cells 48 h after infection with SARS-CoV-2 authentic virus

627   in the presence of increasing concentrations of abovementioned antibodies in their dimeric and monomeric form. (E)

628   Fold improvement of the IC_{50} (upper panel) and IC_{90} (lower panel) values of dimeric IgA to monomeric IgA (X axis)

629   plotted against IC_{50} ($r = 0.6167$, $P = 0.08573$), IC_{90} ($r = 0.4333$, $P = 0.2499$) values of monomeric IgAs. Correlations

630   were analyzed by two-tailed Spearman's tests.

631

632

633

634   **Table S1. Sequences of anti-SARS-CoV-2 antibodies**

635   Auxiliary Supplementary Material.

636

637   **Table S2. Sequences of antibodies from isotype shared clones**

638   Auxiliary Supplementary Material.

639

640   **Table S3. Inhibitory concentrations of monoclonal antibodies from isotype shared clones**

Table S3 Inhibitory concentrations of the monoclonal antibodies from isotype shared clones

Patient ID	IgM	IC50(ng/ml)	IC90(ng/ml)	IgG	IC50(ng/ml)*	IC90(ng/ml)*	IgA	IC50(ng/ml)	IC90(ng/ml)
COV21	-			CG002	8.88	37.61	CA386	5.76	123.33
	-			CG005	60.49	205.20	CA387	9.68	129.87
COV47	-			CG144	6.91	29.66	CA394	13.06	371.86
	CM169	UD	UD	CG148	>1000	>1000	-		
	CM170	5806	37082	CG171	5250	17156	CA457	1721.6	298325.6
	-			CG379	126.98	2368.18	CA403	23.88	126.05
	CM381	UD	UD	CG160	>1000	>1000	-		
	CM349	844.59	26446.73	CG380	2.94	35.96	-		
	CM311	126.85	846.13	CG151	31.79	>1000	CA390	417.42	46597.44
COV96	CM194	UD	UD	CG382	42.92	122.33	-		
	CM365	1226.09	8268.46	CG202	>1000	>1000	-		

UD=Undetectable
*(Robbiani et al. 2020)

641

642   **Table S4. Sequences of cloned recombinant antibodies**

643   Auxiliary Supplementary Material.

644

645   **Table S5. Effective and inhibitory concentrations of monoclonal antibodies**

646   Auxiliary Supplementary Material.

647

648   **Table S6. Inhibitory concentrations of monoclonal IgA monomers and dimers**

Table S6. Inhibitory concentrations of monoclonal IgA monomers and dimers

| Antibody ID | SARS-CoV-2 pseudovirus | | | | SARS-CoV-2 | | | |
| | IC50 (pM) | | IC90 (pM) | | IC50 (pM) | | IC90 (pM) | |
	monomer	dimer	monomer	dimer	monomer	dimer	monomer	dimer
C387	70.68	27.46	543.91	108.06	55.74	11.64	71.46	27.37
C395	74.15	81.64	909.67	239.03	203.72	8.59	769.49	34.10
C399	722.84	47.48	11692.05	339.46	700.38	13.67	2636.98	114.74
C402	2652.52	40.86	15603.86	874.99	1536.24	47.90	4939.53	247.79
C403	3222.29	57.62	19499.80	461.45	491.11	13.18	2115.67	49.85
C404	31112.25	502.11	371134.20	82318.65	6182.08	201.78	18271.60	514.05
C405	27801.09	444.36	294918.48	62867.98	1312.88	78.57	5725.29	266.04
C408	2691.09	147.89	126130.74	1114.44	3392.62	40.51	4458.13	259.84
C437	32.67	41.18	258.08	292.35	13.32	7.84	58.85	21.82

IC50/90 values for dimers were adjusted for number of binding sites

649

650   **Table S7. Primers**

651   Auxiliary Supplementary Material.

652

653

654

655

656